



ASSESSMENT OF COMBINED EFFECTS OF AXIAL AND LATERAL LOADING OF GLUED-IN ROD CONNECTIONS IN LVL

Daniel Fawcett¹, Eleni Toumpanaki²

ABSTRACT: Glued-in rod connections for timber offer improved strength, stiffness, aesthetics and fire performance compared to bolts and dowels. Extensive investigations have been done into the pull-out capacity of rods under pure axial load, however the capacity and stiffness of laterally loaded rods, particularly when combined with axial loading, is under-researched, with further investigation being crucial as nearly all connections are subject to this combination. The provision of an unbonded length has been shown to increase pull-out capacity, but its effect on laterally loaded rods has not been investigated. Investigations also often use softwoods over hardwoods. As a result, design codes lack informed guidance for laterally loaded rods and underestimate the capacity of rods in hardwood. In this study, 15 Beech LVL specimens with steel rods glued in with epoxy adhesive were subjected to varying ratios of axial to lateral load, to study the combined effects. The introduction of lateral load had no effect on axial capacity with a governing failure mode of rod yielding. The lateral capacity exceeded the design code prediction by 92%, and alternative parameters and equations were presented and discussed for more accurate estimation.

KEYWORDS: Glued-in rods, timber, LVL, Eurocode 5, moment rotation, epoxy

1 INTRODUCTION

1.1 GENERAL OVERVIEW OF GLUED-IN RODS

Glued-in rods (GiRs) offer a desirable alternative to bolts and dowels for timber connections [1]. By inserting rods into pre-drilled holes in timber and filling the surrounding void with adhesive to bond them together [2], a very strong and stiff connection is achieved. Multiple rods glued-in at a distance apart provide efficient moment resistance due to the couple of axial forces created [3]. Greater aesthetic appearance and fire resistance is achieved with the timber cover provided, obscuring the rods [4], whereas conventional connections are often exposed or covered with limited wood sheathing.

It is common for steel to be used as the rod material due to its strength and, crucially, ductility. Carbon and glass FRPs [5] and basalt FRP [6] are sometimes used, though despite being very strong and stiff, they lack high ductility.

The adhesives that have been studied for glued-in rods are epoxy, polyurethane and fibre-reinforced phenol-resorcinol, in descending order of strength (determined by the GIROD project in the late 90s [4]). The first two are used most frequently [2].

There are numerous potential modes of failure with this connection type, including longitudinal shear failure in the adhesive, timber-adhesive interface, steel-adhesive interface or in the timber surrounding the adhesive; timber splitting due to short rod-edge or rod-rod distances (particularly with lateral rod loading); or tensile yield failure of the rod or the timber cross-section [2]. The ductile failure mode of steel rod yielding is always preferred over the other brittle failure modes [7]. As a result, all relevant failure modes should be assessed during design, and rod yielding must be the critical one. This requires a detailed understanding of all the failure modes, and how variation of the multitude of parameters involved, including the effect of lateral loading, affects the failure load for each mode.

1.2 RESEARCH INTO GLUED-IN RODS

Many studies have focused just on the ‘pull-out’ capacity of glued-in rods by conduction of tests with the pull-pull test setup (rods glued into both ends of a timber element gripped and pulled apart), as studies can be easily compared if they follow the same experimental programme [8]. Softwoods are often the timber type used for tests, meaning that the current design equations,

¹ Daniel Fawcett, University of Bristol, Department of Civil Engineering, Queen’s Building, University Walk, BS8 1TR, UK, tc19705@bristol.ac.uk

² Eleni Toumpanaki, University of Bristol, Department of Civil Engineering, Queen’s Building, University Walk, BS8 1TR, UK, eleni.toumpanaki@bristol.ac.uk

informed by such tests, often under-predict the pull-out strength of rods glued into hardwoods [9]. In addition, comparatively little research has been done on laterally loaded glued-in rods, let alone combined axial and lateral action. Further research in this area is important as nearly all connections are subject to both axial and lateral force. The provision of an unbonded length close to the loaded end of the rod has been shown to increase the axial pull-out capacity by shifting the longitudinal shear stress distribution in the timber-adhesive interface away from the end grain, where there would otherwise be a local concentration, decreasing the likelihood of timber splitting [2]. Franke et al. [7] showed that an unbonded length of $2d$ prevented timber splitting and reduced experimental scatter, and a greater unbonded length of $5d$ markedly increased the pull-out capacity on top of this. The recently published EN 17334:2021 [10] provides specific guidance for glued-in rod connections regarding universal testing, design, and manufacturing of glued-in rods. Design guidelines for glued-in rods are included in Annex A of [10], which specifies that lateral rod capacity should be estimated using equations for dowel-type fasteners from EC5 [11], which do not have a glue-line. The presence of glue-line can affect the embedment strength of the rods and there is limited research addressing this aspect. Due the current lack of design standards for glued-in rods in EC5 [11], there is still much hesitation in the construction industry over use of glued-in rod connections: a survey [12] found that of the 56 European scientists, timber industrialists and structural designers who took part, 9% use glued-in rods frequently, 68% have never or very rarely used them, 60% are not confident in using them, and 89% are not satisfied with current standards. The second generation of EC5 to be released in 2025 will include design guidelines for bonded-in rods.

1.3 EXISTING STUDIES ON COMBINED AXIAL & LATERAL LOADING

There are limited studies investigating the interaction of axial and lateral rod force in glued-in rods, and these have addressed the brittle failure modes (shear failure in the timber or adhesive, or interfacial shear failure). Aicher and Simon [3] performed tests in spruce glulam GL30h with steel rods of class 8.8 and 16 mm nominal diameter, glued-in with 2 mm thick epoxy resin and parallel to grain. Pull-out tests assessed the axial rod capacities, shear tests assessed the lateral capacities, and cantilever tests assessed the combined axial and lateral interaction, with two different beam lengths tested for different ratios of axial to lateral force. The results, shown in Figure 1, strongly support an elliptic relationship which is given by the current governing equation (Equation (8) in this paper). This study also confirmed that providing greater edge distance between the top rod and top of the timber beam results in a significant increase in the lateral capacity, which is currently not accounted for in design code: rather a minimum edge distance of $4d$ (from the centre of the rod of diameter d) is specified.

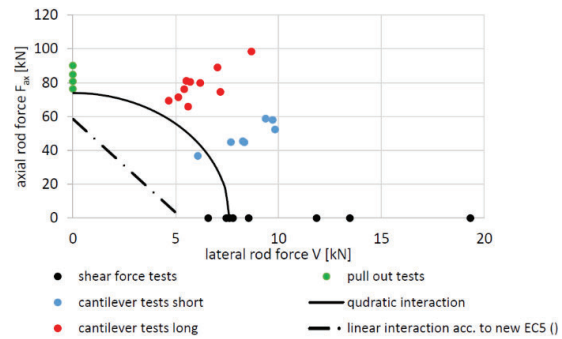


Figure 1: The plotted ultimate rod axial and lateral loads compared to trend lines for Aicher's and Simon's study [3].

This minimum edge distance was used for some specimens and the results were close to the EC5 [11] prediction.

Walker and Xiao [13] performed tests with a different setup, whereby rods were glued-in at differing angles to the timber surface but still parallel to grain, as indicated by Figure 2, and pulled out with force normal to the timber surface, inducing a lateral force component in the rotated section of the rod. The timber was LVL, and the bent rods were class 8.8 steel of 12 mm nominal diameter, bonded with 4 mm glue-line thickness. Contrary to the previous study, this yielded a decreasing linear interaction between the axial and lateral rod force, as depicted in Figure 3. Reasons could include the different test method or the different materials.

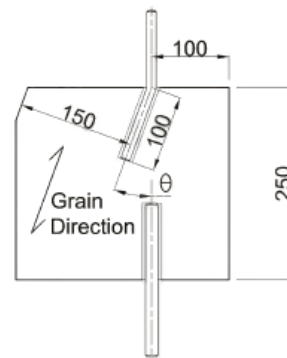


Figure 2: The setup of Walker's and Xiao's study [13].

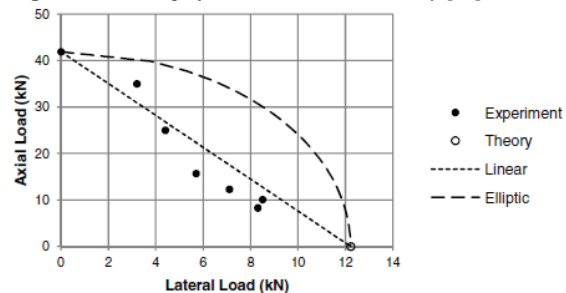


Figure 3: The plotted ultimate rod axial and lateral loads compared to trend lines for Walker's and Xiao's study [13].

2 DESIGN EQUATIONS & CRITICISMS

2.1 AXIAL CAPACITY

EN 17334 A.2.4 [10] specifies the axial capacity of glued-in steel rods as given by Equation (1):

$$F_{ax,Rd} = \min \left\{ \begin{array}{l} f_{y,d} A_{ef} \\ \pi d l_a f_{vr,d} \end{array} \right. \quad (1)$$

where $F_{ax,Rd}$ is the rod axial capacity (N), $f_{y,d}$ is the design yield strength of the steel rod (N/mm²), A_{ef} is the effective stress area of the rod (mm², equal to the nominal stress area $A_{s,nom}$ specified in [14]), d is the nominal rod diameter (mm), l_a is the bond length (mm), and $f_{vr,d}$ is the design adhesive bond strength (N/mm²). The two expressions are for the rod yield and adhesive ('pull-out') capacity respectively. Equation (1) is widely used and included in other design codes. However, it does not account for the fact that increasing bond length provides diminishing (not linear) returns for increased capacity, which has been shown by many studies [2].

2.2 LATERAL CAPACITY

For calculation of rod lateral capacity, EN 17334 A.3.1 and A.3.2 [10] specify referral to sections 8.2 and 8.5 of EC5 [11] respectively, which give design equations for the lateral capacity of metal dowel-type fasteners. The lateral capacity of a metal dowel-type fastener (or in this case the glued-in rod) connected to a thin plate in single shear is given by Equation (2):

$$F_{v,Rk} = \min \left\{ \begin{array}{l} 0.4 f_{h,k} t_1 d \\ 1.15 \sqrt{2 M_{y,Rk} f_{h,k} d + \frac{F_{ax,Rk}^2}{4}} \end{array} \right. \quad (2)$$

where $F_{v,Rk}$ is the characteristic fastener (rod) lateral capacity (N), $f_{h,k}$ is the characteristic timber embedment strength (N/mm²), t_1 is equal to the bond length l_a (mm) for glued-in rods, d is the nominal fastener (rod) diameter (mm), $M_{y,Rk}$ is the characteristic fastener (rod) yield moment (Nmm), and $F_{ax,Rk}$ is the fastener (rod) axial capacity (N). Alternatively, the lateral capacity for connections to a thick plate in single shear is given by Equation (3):

$$F_{v,Rk} = \min \left\{ \begin{array}{l} f_{h,k} t_1 d \\ f_{h,k} t_1 d \left(\sqrt{2 + \frac{4 M_{y,Rk}}{f_{h,k} d t_1^2}} - 1 \right) + \frac{F_{ax,Rk}}{4} \\ 2.3 \sqrt{M_{y,Rk} f_{h,k} d + \frac{F_{ax,Rk}^2}{4}} \end{array} \right. \quad (3)$$

Each expression within Equations (2) and (3) is for a different failure mode, with Figure 4 illustrating them. The first terms are the capacities according to Johansen yield theory, and the second term $F_{ax,Rk}/4$ included in some of the expressions is an estimation of the beneficial contribution from the rope effect. EC5 [11] section 8.2.2(2) specifies different limits for the contribution of

this effect, as a percentage of the Johansen part, for different fastener types. A 25% limit for bolts was applied for estimated lateral rod capacities in this study, and the appropriateness of this value for glued-in rods was discussed upon analysis of the experimental results.

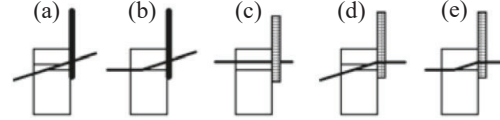


Figure 4: Depicted failure modes from Equations (2) and (3), in the same order the expressions are in (from Figure 8.3 of EN 1995-1-1:2004).

The embedment strength parallel to grain is given by equation 8.32 in section 8.5.1.1 of EC5 [11]. EN 17334 A.3.4 and A.3.5 [10] combined specify a factor of 0.125 on this to give the embedment strength perpendicular to grain, $f_{h,90,k}$, given in Equation (4), which is applicable for laterally loaded rods glued-in parallel to grain:

$$f_{h,90,k} = 0.125 \cdot 0.082(1 - 0.01d) \rho_k \quad (4)$$

where ρ_k is the characteristic timber density (kg/m³). Equation (4) doesn't account for the use of an EWP (e.g. glulam or LVL) over sawn timber, or for the presence of adhesive. The embedment strength of the adhesive and timber in combination and the glue-line thickness are not considered. An effective density equal to the geometric mean of the timber and adhesive densities, given in Equation (5), could be used in place of ρ_k in Equation (4) to calculate the embedment strength required for Equations (2) or (3):

$$\rho_{ef} = \sqrt{\rho_{timber} \cdot \rho_{adhesive}} \quad (5)$$

Furthermore, none of the previous discussion accounts for the presence of an unbonded zone. The absence of adhesive near the shear plane results in a gap around the rod, causing the rod to bend and embed directly into the above timber, affecting the failure mode and capacity. Moreover, the bearing zone is lower than the theoretical one including part of the unbonded length due to the local restrictive effect of the fully bonded length (see Figure 5).

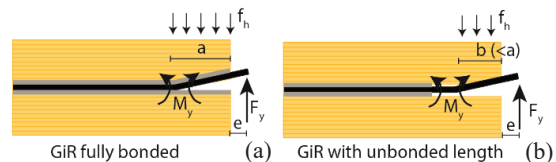


Figure 5: Embedment stresses in (a) a fully bonded glued-in rod and in (b) a glued-in rod with an unbonded length.

Riberholt [15] proposed equations to estimate the timber embedment strength and lateral capacity for laterally loaded glued-in bolts, with consideration of the bolt and

hole diameters (the maximum of which is d (mm)), bolt yield moment M_y (Nmm), embedment strength f_h (N/mm²) and eccentricity, e , of the applied lateral load with respect to the timber loaded face (mm) where there is absence of bearing stresses. The maximum lateral force F (N) acting at distance e is given by Equation (6):

$$F = \left(\sqrt{e^2 + \frac{2M_y}{df_h}} - e \right) df_h \quad (6)$$

with embedment strength f_h given by Equation (7):

$$f_h = (2.3 + 750d^{-1.5})\rho \quad (7)$$

where ρ is the relative timber density (dimensionless, normalised by $\rho_{water} = 1000 \text{ kg/m}^3$). Equation (6) accounts for both bolt (rod) yielding and embedment failure. It may appear sensible at first to assign the unbonded length as the load eccentricity, e , as the rod is not supported over this length. However, it will likely not take much rod deformation until the rod contacts with the timber at the end of the unbonded zone, i.e. yield failure in the rod won't yet have occurred. This contact then means more support to resist rod yielding due to bending, and likely embedment failure here instead of at the end of the bonded zone, not predicted by Equations (6) and (7). Furthermore, the equations do not account for thick glue-lines and are derived for glulam, whereas LVL is likely to have greater embedment strength (discussed later). Clearly a new and more comprehensive set of equations is needed. Nevertheless, Equations (6) and (7) were also used to give a prediction of the lateral load capacity.

2.3 AXIAL & LATERAL COMBINED CAPACITY

EN 17334 A.4 [10] recommends an elliptic relationship between the axial and lateral rod forces, given in Equation (8), to be satisfied:

$$\left(\frac{F_{lat,Ed}}{F_{lat,Rd}} \right)^2 + \left(\frac{F_{ax,Ed}}{F_{ax,Rd}} \right)^2 \leq 1 \quad (8)$$

This equation is found in other design codes such as DIN EN 1995-1-1/NA [16], in addition to a linear version (the quotient terms not squared) given in the Final draft *Connections SC5.T5* to the new DIN EN 1995-1-1:2020 [3]. The results of Aicher and Simon [3] support the elliptic relationship, whereas the results of Walker and Xiao [13] support the linear relationship.

2.4 ROTATIONAL STIFFNESS

There are no standards for the estimation of the rotational stiffness of timber connections [17], but such calculations are important for serviceability checks. As such, analytical models are proposed in literature, and they are verified with experiments. This study makes use of the proposal by [18]: a component method for moment-resisting glued-in steel rod connections in glulam, analogous to that used for steel moment connections. It is

recommended to refer to their paper for the full set of equations involved and the supporting diagrams, though an equation of interest is the stiffness of the timber compression zone k_c (N/mm), given by Equation (9):

$$k_c = \frac{E_{w,0}\sqrt{A_c}}{4} \quad (9)$$

where $E_{w,0}$ is the timber elastic modulus parallel to grain (N/mm²) and A_c is the area of timber in compression (mm²). Equation (9), as derived from equation 17 in [18], has been modified here so that it is applicable to the specimens in this study, due to differences in the type of support. Note how there is no inclusion of the timber beam length: this is discussed in section 4.4.

To calculate the rod axial stiffness, required for the above model, Xu et al. [1] proposes using the axial rigidity $E_s A_s$ (N) divided by the bond length l_a (mm), but with the addition of a coefficient 0.3 to account for mechanical interlocking and the bond stress distribution along the bonded length, hence providing an effective stiffness. This coefficient value was determined by comparison between FE analysis and an experiment on the same specimen. Deviations due different materials (e.g., glulam versus LVL) and adhesive types may lie between studies. The steel rod stiffness k_s (N/mm) is hence given by Equation (10):

$$k_s = \frac{E_s A_s}{0.3l_a} \quad (10)$$

2.5 OUTLINE OF THIS STUDY

The purpose of this study was to investigate the effects of combined axial and lateral force in the axial withdrawal capacity of glued-in rods in LVL. The study addresses the ductile failure mode for glued-in rods (rod steel yielding) as opposed to the brittle failure modes that have been investigated in other studies. This is because the steel yielding failure mode is the expected design failure mode, to increase ductility and energy dissipation, and favour load re-distribution and non-catastrophic sudden failures. For the evaluation of the axial and lateral load capacities, pull-pull and shear tests were conducted respectively. The combined effects of axial and lateral loading were investigated with cantilever tests of varying length, similar to the test methodology in [3]. The EN 17334 [10] design rules were adhered to, and its design capacity equations were used as the baseline comparison for the results of the study. A fixed unbonded length was provided for all specimens to investigate the resulting effect on the rod capacities when compared to predictions. The axial and rotational stiffnesses of the connections were also measured experimentally and compared to predictions using the analytical models discussed in previous section. Characteristic values (rather than design values) were used.

3 EXPERIMENT PROGRAMME

3.1 MATERIALS

Steel rods with a metric thread, a nominal diameter of 12 mm and of property class 8.8 were used, hence they had characteristic yield strength $f_{y,k} = 640 \text{ N/mm}^2$, tensile strength $f_{u,k} = 800 \text{ N/mm}^2$ and nominal stress area $A_{s,nom} = 84.3 \text{ mm}^2$ [14]. The yield and tensile strengths of the three steel rods were verified by tensile tests. The results were a mean 0.2% proof stress of 613.0 N/mm^2 (standard deviation 14.3 N/mm^2) and a mean tensile strength of 783.0 N/mm^2 (standard deviation 9.2 N/mm^2), respectively 4.2% and 2.1% lower than the respective characteristic strengths. The experimental values were used in the design equations for rod capacities rather than the characteristic strengths given in [14]. An elastic modulus of 200 kN/mm^2 was assumed for the rods. The timber was Beech LVL (BauBuche GL70). An average moisture content of 13.5% was recorded after testing with a Protimeter Surveymaster Moisture Meter using the non-invasive method. Tests on the same timber in [19] yielded a flexural elastic modulus of 15.7 kN/mm^2 and a compressive yield stress of 43 N/mm^2 . The adhesive used was a 2-component thixotropic epoxy adhesive (Rotafix Timberset Adhesive), especially suited to bonding metal to timber, with a bond strength of 6-10 N/mm^2 according to the manufacturer, with $>6 \text{ N/mm}^2$ specified for UK structural softwoods and $>9 \text{ N/mm}^2$ for Jarrah hardwood [20].

3.2 SPECIMEN GEOMETRIES & SETUPS

The specimen geometries and test arrangements are summarised in Figure 6, with the actual specimens shown in Figure 7. The nomenclature adopted is S for shear tests, A for axial pull-pull tests and C for cantilever tests with 1, 2 and 3 referring to a specimen length of 500, 750 and 1000 mm respectively. Three specimens were tested for each test configuration, hence a total of 15. The bond length was fixed at 240 mm, with an unbonded length of 50 mm (the maximum according to [10]) provided for all specimens by wrapping duct tape around the rods in this region to stop adhesive flow encroaching in the unbonded length during manufacturing of the specimens. The rod hole diameters were 16 mm, yielding a 2 mm glue-line thickness. The adhesive was applied by injection and exit through 2 respective pre-drilled holes of 8 mm diameter perpendicular to the rod hole, with the rods inserted beforehand and aligned with acrylic rings. This method of adhesive application ensures minimal skew in rod alignment and good filling of voids with adhesive, providing some quality assurance [2]. Rod lengths, separations and edge distances all complied with rules in [10], such as the minimum top rod edge distance of $4d$ provided for all tests (except the axial tests which had greater edge distance).

3.3 AXIAL (PULL-PULL) TESTS

The axial specimens were subjected to ‘pull-pull’ tests to study axial behaviour without the influence of lateral load. The test setup is shown in Figure 8(a). The axial

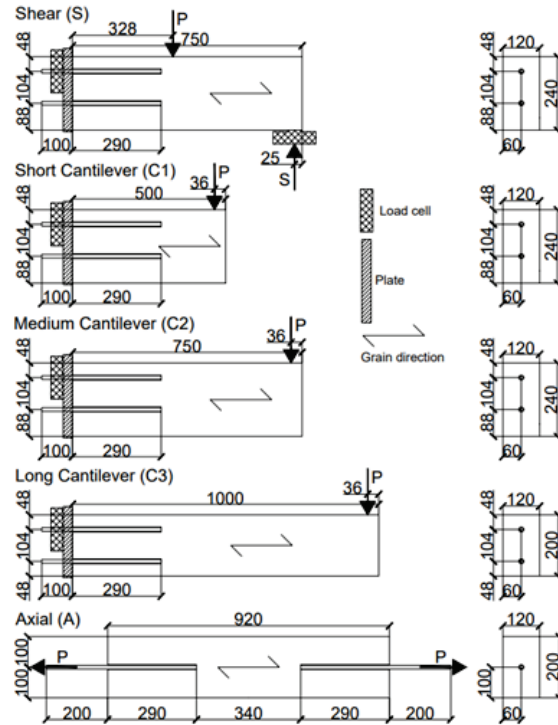


Figure 6: Summary of the specimen geometries and test setups.



Figure 7: Specimens following the application of the adhesive.

displacement of the rods was tracked by 2 LVDTs on either side (for the mean average). The test was conducted at a displacement control mode of 1 mm/min.

3.4 CANTILEVER TESTS

The setup for the cantilever tests is shown in Figure 8(b). The large supporting plate was 30 mm thick ($>d$ hence thick according to [11]). No separation was provided between the timber face and supporting plate for these tests, to mimic the realistic situation of a timber beam connected to a steel connector plate. As a result, a compressive distribution was to be introduced into the timber. Analytical equations derived in [21] were used to

estimate the position of the neutral axis of bending, which was found to be below the bottom rod for all cantilever specimens. As a result, the bottom rod was predicted to also experience tension, though much less than the top rod. For the cantilever (and shear) tests, a pancake load cell tracked the tension force in the top rod (the expected failure region). Even distribution of lateral force between the rods was assumed, as verified with a FE model in the linear elastic range, so the individual lateral rod forces were taken to be half of the total (equal to the specimen weight plus the applied load P).

Axial displacements of the rods were again tracked by 2 LVDTs either side of each rod (for the mean average). The load, P , was applied at 3-7 mm/min downward displacement (the longer the cantilever the higher the displacement rate).

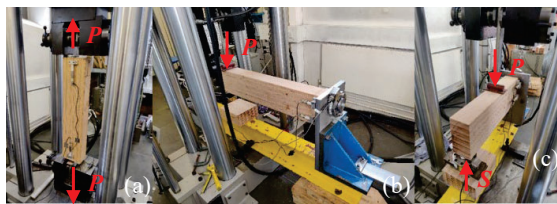


Figure 8: (a) The axial, (b) cantilever and (c) shear test setups.

3.5 SHEAR TESTS

The setup for the shear tests is shown in Figure 8(c). The shear test setup involved a slight adaptation to the cantilever test setup, with a support provided under the (previously) free end (of which the load taken, S , was tracked with a pancake load cell), and with load P applied just beyond the end of the bond zone of the rods: a compromise between applying load close to the support to minimise moment hence axial rod load in that region (as these tests are an investigation of the lateral capacity), and applying load away from the end of the rods to avoid interfering with their failure. Separation was provided between the timber and supporting plate with washers in these tests to eliminate steel-timber friction, for accurate tracking of the total lateral rod loads, equal to the specimen weight plus the applied load, P , minus the support load, S . The load, P , was applied at 2 mm/min downward displacement.

4 RESULTS AND DISCUSSION

4.1 AXIAL & CANTILEVER SPECIMEN RESULTS (AXIAL CAPACITY & STIFFNESS)

The results for the rod forces and slippages are summarised in Table 1. Only results for the top rods are shown as failure always occurred here. Note that the ‘failure’ yield point is top rod yielding for the A and C1-3 specimens, and first crack for the S specimens; and the ‘ultimate’ load point is the maximum top rod load reached for the A and C1-3 specimens, and the first significant split for the S specimens. One of the C1 specimens failed prematurely (short of top rod yielding) due to a connection issue, hence data from this test was only used for rotational stiffness assessment. One test from the C2 and

C3 group stopped prematurely at the ultimate load due to a hydraulics issue.

Examples of the observed failures are shown in Figure 9. The failure mode for all tests, except the shear tests, was yielding of the steel rods at 51.7 kN according to the experimental yield strength value. The predicted failure loads according to Equation (1) range from 54.3-90.5 kN (for adhesive bond strength 6-10 N/mm², see section 3) with the lowest value corresponding to steel yielding based on the nominal yield strength. Most specimens reached ultimate load followed by fracture, with a mean ultimate load reached at 64.2 kN for the axial and cantilever specimen top rods (4.7% lower than the nominal value of 67.4 kN). The yield (and consequently fracture) points often occurred in the unbonded zone within the timber. The mean ultimate load value suggests an adhesive bond strength of >7.1 N/mm², as no signs of failure of the adhesive were observed.

The LVDT data confirmed tension in the bottom rods for the cantilever tests, with its value estimated by subtracting the measured top rod force from the timber compressive force, which was estimated with Euler-Bernoulli theory. The timber compression was very large, commonly reaching around 112 kN for the C1 and C2 tests, and the resulting extreme fibre compressive stress reached around 35 N/mm², below the compressive yield stress of 43 N/mm² [19].

Table 1: Mean average values for load and slip at failure for top rods, and axial stiffness (outliers excluded; bracketed values are ultimate; non-bracketed values are at yield or first crack for S specimens)

Specimen	Axial Load (kN)	Lateral Load (kN)	Axial Slip (mm)	Axial Stiffness (kN/mm)
S	14.1 (14.6)	18.4 (18.7)	-	-
C1	51.7 (62.5)	14.4 (18.6)	1.1	13.4 (17.3)
C2	51.7 (64.5)	9.0 (12.2)	1.2	12.8 (17.4)
C3	51.7 (64.2)	4.4 (6.1)	1.1	8.4 (11.7)
A	51.7 (65.1)	0.0 (0.0)	0.7	-

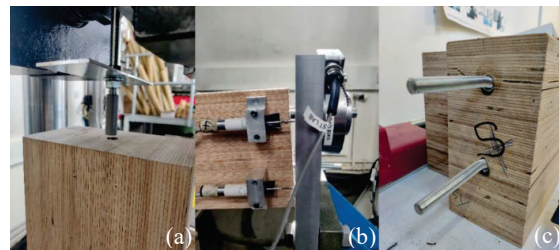


Figure 9: Typical failures: (a) tensile failure after steel yielding in axial specimens, (b) tensile failure after steel yielding in cantilever specimens, and (c) rod deformation, embedment failure and LVL splitting in shear specimens.

Figures 10-13 are the graphs of the top rod axial load against rod axial displacement for the axial and cantilever tests. The graphs each show 2 series of results: one corrected for the elastic rod strain (between the end of the bond zone and the nuts used to secure them behind the steel plate) up to the yield load, hence giving the relationship between rod load and rod slippage; and the other showing the full displacements including the region of plastic behaviour (elastic, plastic and slippage displacements; grey plots).

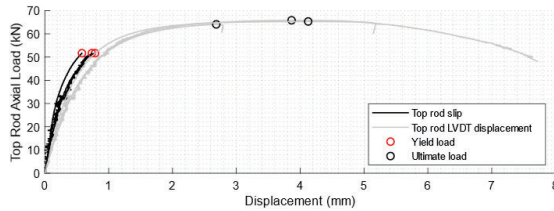


Figure 10: Top rod axial force-slip and full axial force-displacement curves for the axial (A) tests.

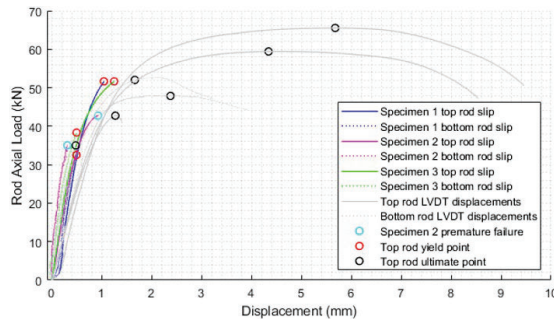


Figure 11: Top and bottom rod axial force-slip and full axial force-displacement curves for the short cantilever (C1) tests.

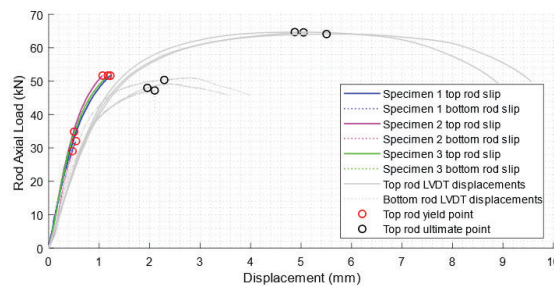


Figure 12: Top and bottom rod axial force-slip and full axial force-displacement curves for the medium cantilever (C2) tests.

The axial stiffnesses of the top rods were calculated using the linear elastic range of the load-slip relationship, assumed to be between 10-40% of the ultimate rod load, with the values given in Table 1, as well as the slippage values at yield failure. The cantilever specimen top rod stiffnesses (which were very similar despite differing lateral load) were an average of 43% lower than the axial specimen rod stiffnesses (79.0 kN/mm compared to 138.6 kN/mm), indicating that a small addition of lateral load due to cantilever action markedly decreases the axial stiffness, though internal timber strain differences due

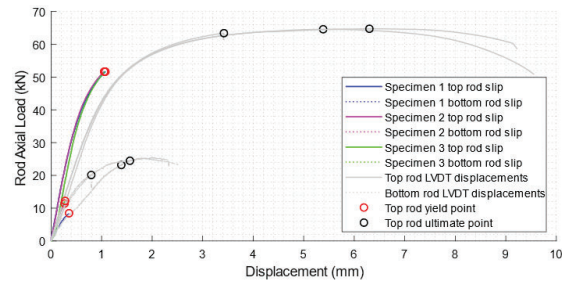


Figure 13: Top and bottom rod axial force-slip and full axial force-displacement curves for the long cantilever (C3) tests.

to different rod edge distances and timber areas could also contribute to this.

An interesting observation is how the total lateral forces in the short cantilever tests were only slightly less than those in the shear tests, but no signs of splitting or embedment failure were observed. A reason could be the yielding of the top rod combined with increased embedment stresses leading to load redistribution to the bottom rod, causing neither to quite reach the lateral load capacity. Another likely reason could be a vertical frictional resistance introduced due to the timber-steel contact which, if accounted for (assuming a friction coefficient of 0.2 [22]), is found to be dominant, given the large timber compression force. However, this friction force is expected to be limited given the small hole clearance in the steel plate, and the main bearing action between the rods and the plate. The friction force was not included in the results due to its uncertain value and variation, but its presence can represent a real scenario of a moment resisting connection.

4.2 SHEAR SPECIMEN RESULTS (LATERAL CAPACITY)

The shear specimens failed by splitting of the LVL in lamination plane interfaces around the top rod, as shown in Figure 9 (c). Embedment failure was observed at the end of the unbonded zone as predicted, due to the upward rod deformation which the zone allowed for. The rod deformations and embedment failures were greater in the bottom rods, though this could be due to a transfer of much of the lateral load to the bottom rod upon splitting failure around the top rod, rather than an uneven force distribution between the rods throughout the test within the linear elastic range.

Calculations using the measured P and S forces confirmed an increasing sagging moment at the rod support for the duration of all 3 shear tests, likely as this end displaced downwards due to rod deformation and embedment failure, but the other end was vertically restrained due to the rigid vertical support provided by the pancake load cell. Such behaviour is expected with plastic hinge formation at the rod support. The top rods experienced axial tension of 23-34% of the yield load, as measured by the pancake load cell, with loads shown in Figure 14. A likely reason could be a significant axial force due to the rope effect, evidenced by the large deformation of the rods observed, causing them to be 'pulled through' the plate.

Such a force would significantly exceed the 25% limit prescribed for the contribution to the lateral capacity of bolts, used to estimate the rod lateral capacities in this study, indicating that a higher limit (the determination of which requires further investigation) may be more suitable for glued-in rods.

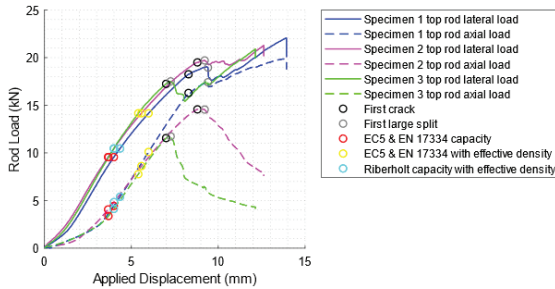


Figure 14: Graph of top rod loads against the vertical displacement at the point of load application for the shear (S) tests, with predicted and observed failure loads indicated.

Table 1 includes the lateral force values at failure, with a mean of 18.4 kN observed. Referring back to section 2.2, use of EC5 [11] equations yield an embedment strength of 6.1 N/mm² (Equation (4)), and hence a lateral capacity of 9.6 kN according to the failure mode (c) of Equation (3) (as the plate used was thick), which is 92% less than the observed lateral capacity. This disparity is attributed to the use of LVL causing an under-prediction of the embedment strength, and the provision of an unbonded length, which shifts the lateral force distribution away from the timber surface, hence increasing the resistance to splitting. Equation (4) does not account for use of an EWP over sawn timber, with LVL being particularly neglected due to the thinner laminations (as opposed to glulam). Schweigler et al. [23] found an embedment strength of 27.5 N/mm² for dowels in LVL (of the same 12mm diameter of the rods used in this study), which is 351% greater than the EC5 [11] predicted value; similarly, Bader et al. [24] found 24.9 N/mm². Using $f_{h,k} = 27.5$ N/mm² for Equation (3) yields a much greater capacity of 19.5 kN (again from the bottom expression), which is close to the observed capacity, but does not account for the presence of the adhesive or unbonded length. Alternatively, using an effective density according to Equation (5), with $\rho_{timber} = 680$ kg/m³ for GL70 BauBuche LVL [25], and $\rho_{adhesive} = 3125$ kg/m³ [20], $\rho_{ef} = 1458$ kg/m³ is yielded, hence an increased embedment strength of 13.2 N/mm² and an increased capacity of 14.1 kN. Riberholt's [15] proposal yields a lateral capacity of 2.6 kN if Equation (7) is adopted in Equation (6) based on the timber density. This results in a vast underprediction. If the effective density, ρ_{ef} (converted to relative for Equation (7)) is adopted, this yields a high embedment strength of 29.7 N/mm², thus a lateral capacity of 10.5 kN. This is slightly greater than the EC5 [11] and EN 17334 [10] prediction, but it is still only 57% of the experimental lateral capacity. In the previous calculations, e is set to equal 0, such that the embedment strength at the end of the bond zone is estimated. It should be noted that

Equations (6) and (7) were derived from fully bonded rods and some deviations are expected due to the non-uniform embedment stresses when an unbonded length is provided.

4.3 COMBINED AXIAL & LATERAL FORCE INTERACTION

Figure 15 shows the experimental data of axial and lateral loads for all specimens (top rods only), compared to the elliptic design capacity relationships (Equation (8)) using the various lateral capacities discussed previously. For the Riberholt capacity using Equation (6), only the effective density was considered. It is evident that there is no relationship between axial load capacities and lateral loads when rod yielding is the dominant failure mode, as the elliptic trend is not followed (as opposed to pull-out failure, for which Aicher and Simon [3] confirmed suitability of the elliptic relationship). This is particularly evident for the short cantilever tests, where the failure loads far exceed the EC5 [11] and EN 17334 [10] design capacity line. The experimental lateral load capacities (from the shear tests) agreed well with the EN 17334 [10] design prediction when a higher embedment strength of 27.5 N/mm² was used. The effect of lateral loads in ductile failure modes of glued-in rods should be directly addressed in the current design guidelines.

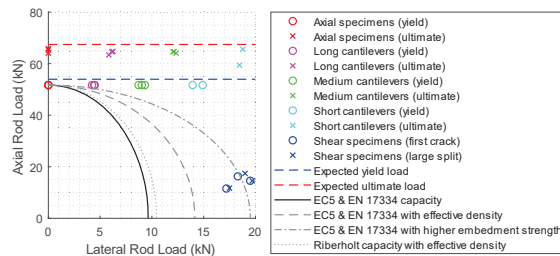


Figure 15: Graph of axial load against lateral load for the failure and ultimate points for all specimens, with prescribed and suggested elliptic trend lines for load limits also plotted.

4.4 MOMENT-ROTATION RESULTS

The cantilever specimen support moment and rotation results are summarised in Table 2, in addition to theoretical stiffnesses calculated using the model discussed in section 2.4. The support rotations were derived from the LVDT data for the top rod (combined rod strain and slip) and the predicted strain of the extreme timber compression fibre. In the calculations the weight of the beam was also considered. The moment-rotation relationships are plotted in Figure 16, along with the theoretical predictions. The rotational stiffnesses were calculated using the linear range of the moment-rotation relationships, ranging from 10-40% of the ultimate moment. The mean experimental rotational stiffness of the C1 specimens was 10.7% higher than that of the C2 specimens despite the same predicted stiffness, attributed potentially to an influence of the beam length that is not accounted for by the analytical model used (the C1 specimen length being 33.3% shorter than the C2 length),

though this difference could be insignificant considering experimental scatter.

Table 2: Mean average values for support moment and rotation at failure (bracketed values are ultimate; non-bracketed values are at yield); and rotational stiffnesses.

Specimen	Support Moment (kNm)	Support Rotation (mrad)	Experiment Rotational Stiffness (kNm/rad)	Theoretical Rotational Stiffness (kNm/rad)
C1	13.4 (17.3)	9.56	1870	1980
C2	12.8 (17.4)	9.55	1690	1980
C3	8.4 (11.7)	11.15	950	1120

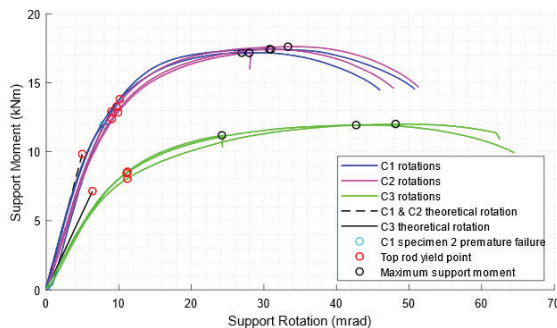


Figure 16: Moment-rotation curves for the cantilever specimens, with theoretical rotations also plotted.

The experimental rotational stiffnesses are always lower than the theoretical ones: for a two-tailed t-test with 5% significance, the results for the C1 tests are not statistically significant, but the results for the C2 and C3 tests are. A higher coefficient on the bond length for a greater effective stiffness length (as opposed to 0.3 as discussed in section 3.4) may be more appropriate, given that different timber and adhesive is used here than in [1], where glulam and a different epoxy adhesive were investigated. A coefficient of 0.9 is found to result in a similar axial stiffness to those observed in the cantilever tests. It is also observed that top rod yielding occurs at greater support moment and rotation than predicted.

5 CONCLUSIONS

The application of lateral load to the rods had no effect on their axial capacities with a governing failure mode of rod yielding; this should be addressed in the design guidelines. The lateral capacities of the shear specimens exceeded the design code prediction by 92%, and the use of an effective density accounting for the presence of adhesive in calculation of the embedment strength was shown to give a better prediction. The use of a higher embedment strength for LVL found from literature (27.5 N/mm² as opposed to just 6.1 N/mm² as predicted by EC5 [11], which is a staggering 351% lower) was shown to predict the lateral capacity very accurately, but it did not

account for the adhesive or unbonded length. An unexpectedly significant axial force due to the rope effect was observed for the shear specimens, exceeding the 25% design limit, hence a higher limit for glued-in rods may be appropriate. Axial rod stiffnesses decreased by 43% with a small addition of lateral load due to cantilever action, with the quantity of load not having a notable further effect. Cantilever rotational stiffness was always slightly lower than the theoretical prediction, and a lower stiffness was observed for longer beams but of the same cross-section, which the analytical model used did not account for.

It is of interest to investigate the effect of lateral load on the axial load capacities of steel rods glued into LVL for the brittle failure modes, and understand in depth the lateral load distribution between rods when yielding or first failure occurs in the top rod. A comparison between fully bonded glued-in rods and glued-in rods with an unbonded length will shed more light on the effect of the unbonded length in the embedment stress distribution of GiRs when subjected to lateral loads. This can lead to updates regarding design equations for the lateral load capacity of GiRs with the presence of a glue-line and an unbonded length.

ACKNOWLEDGEMENT

Acknowledgement is given to Joshua Mudie who sourced the LVL for their project [19] and who's supervisor, James Norman, gave permission for the use of the left-over LVL for this project; and to the staff at the University of Bristol's Mechanical Workshop and Heavy & Light Structures Lab for their assistance with the manufacture and testing (respectively) of the specimens.

REFERENCES

- [1] Xu B. H., Bouchair A., Racher P.: Analytical study and finite element modelling of timber connections with glued-in rods in bending. *Construction and Building Materials*, 34:337-345, 2012.
- [2] Steiger R., Serrano E., Stepinac M., Rajcic V., O'Neill C., McPolin D., Widmann R.: Strengthening of timber structures with glued-in rods. *Construction and Building Materials*, 97:90-105, 2015.
- [3] Aicher S., Simon K.: Rigid Glulam Joints with Glued-in Rods subjected to Axial and Lateral Force Action. In *Proceedings of INTER 2021: The 8th Meeting of the International Network on Timber Engineering Research*, 2021. Timber Scientific Publishing, KIT Holzbau und Baukonstruktionen, Reinhard-Baumeister-Platz 1, 76131 Karlsruhe, Germany, 113-128.
- [4] Tlustochowicz G., Serrano E., and Steiger R.: State-of-the-art review on timber connections with glued-in steel rods. *Materials and Structures*, 44(5):997-1020, 2011.
- [5] Toumpanaki E., Ramage M. H.: Glued-in CFRP and GFRP rods in block laminated timber subjected to monotonic and cyclic loading: *Composite Structures*, 272:114201, 2021.

- [6] O'Neill C., McPolin D., Taylor S. E., Martin T., Harte A. M.: Glued-in basalt FRP rods under combined axial force and bending moment: An experimental study. *Composite Structures*, 186:267-273, 2018.
- [7] Franke S., Heubuch S., Franke B.: Glued-in Rods in Beech GLT - Investigation of Pull-Out Resistance and Design Proposal. In *Proceedings of WCTE 2020: World Conference on Timber Engineering*, Santiago, Chile, 2020.
- [8] Steiger R., Gehri E., Widmann R.: Pull-out strength of axially loaded steel rods bonded in glulam parallel to the grain. *Materials and Structures*, 40(1):69-78, 2007.
- [9] Ogrizovic J., Wanninger F., Frangi A.: Experimental and analytical analysis of moment-resisting connections with glued-in rods. *Engineering Structures*, 145:322-332, 2017.
- [10] BSI: EN 17334. Glued-in rods in glued structural timber products. Testing, requirements and bond shear strength classification. British Standards Institute, London, United Kingdom, 2021.
- [11] BSI: EN 1995-1-1. Eurocode 5: Design of timber structures. General. Common rules and rules for buildings. British Standards Institute, London, United Kingdom, 2004.
- [12] Stepinac M., Rajcic V., Hunger F., van de Kuilen J. W. G.: Glued-in rods in beech laminated veneer lumber. *European Journal of Wood and Wood Products*, 74(3):463-466, 2016.
- [13] Walker J., Xiao R.: Experimental Testing of a Portal Frame Connection Using Glued-In Steel Rods. In *Proceedings of the RILEM International Symposium on Materials and Joints in Timber Structures*, Stuttgart, Germany, 2013 (Aicher S, Reinhardt HW and Garrecht H (eds)). RILEM Bookseries, vol. 9, pp. 555-566, 2014.
- [14] BSI: EN ISO 898-1. Mechanical properties of fasteners made of carbon steel and alloy steel. Bolts, screws and studs with specified property classes. Coarse thread and fine pitch thread. British Standards Institute, London, United Kingdom, 2013.
- [15] Riberholt H.: Glued Bolts in Glulam - Proposals for CIB Code. In *Proceedings of the CIB-W18 Meeting 21*, paper 21-7-2, Parksville, Vancouver Island, Canada, 1988.
- [16] DIN: EN 1995-1-1/NA. National Annex - Nationally determined parameters - Eurocode 5: Design of timber structures - Part 1-1: General - Common rules and rules for buildings. Deutsches Institut für Normung, Berlin, Germany, 2013.
- [17] Johanides M., Mikolasek D., Lokaj A., Mynarcik P., Marcalikova Z., Sucharda O.: Rotational Stiffness and Carrying Capacity of Timber Frame Corners with Dowel Type Connections. *Materials*, 14(23): Article No. 7429, 2021.
- [18] Yang H., Liu W., Ren X.: A component method for moment-resistant glulam beam-column connections with glued-in steel rods. *Engineering Structures*, 115:42-54, 2016.
- [19] Sebastian W. M., Mudie J., Cox G., Piazza M., Tomasi R., Giongo I.: Insight into mechanics of externally indeterminate hardwood-concrete composite beams. *Construction and Building Materials*, 102:1029-1048, 2016.
- [20] Rotafix: Rotafix Timberset Adhesive, n.d. See: <http://rotafix.co.uk/products/timber-engineering/rotafix-timberset-adhesive/> (accessed 10/04/2022).
- [21] Fragiacommo M., Batchelar M.: Timber Frame Moment Joints with Glued-In Steel Rods. I: Design. *Journal of Structural Engineering*, 138(6):789-801, 2012.
- [22] McKenzie W. M., Karpovich H.: The frictional behaviour of wood. *Wood Science and Technology*, 2:139-152, 1968.
- [23] Schweigler M., Bader T. K., Hochreiner G., Unger G., Eberhardsteiner J.: Load-to-grain angle dependence of the embedment behavior of dowel-type fasteners in laminated veneer lumber. *Construction and Building Materials*, 126:1020-1033, 2016.
- [24] Bader T. K., Schweigler M., Serrano E., Dorn M., Enquist B., Hochreiner G.: Integrative experimental characterization and engineering modeling of single-dowel connections in LVL. *Construction and Building Materials*, 107:235-246, 2016.
- [25] Pollmeir: Declaration of performance, 2015. See: https://www.pollmeier.com/dam/jcr:98e30343-0ab1-4b41-999f-dd04d3bda04b/EN_Declaration%20of%20performance_beam%20GL70_PM-004-2015.pdf (accessed 14/04/2022).